IEEE Access
Multidisciplinary | Rapid Review | Open Access Journal

Received April 9, 2019, accepted April 25, 2019, date of publication April 29, 2019, date of current version May 14, 2019.

Digital Object Identifier 10.1109/ACCESS.2019.2914002

Distribution of the Residual Self-Interference Power in In-Band Full-Duplex Wireless Systems

LUIS IRIO AND RODOLFO OLIVEIRA, (Senior Member, IEEE)
Instituto de Telecomunicações, 1049-001 Lisbon, Portugal
Departamento de Engenharia Electrotécnica, Faculdade de Ciências e Tecnologia, FCT, Universidade Nova de Lisboa, 2829-516 Caparica, Portugal

Corresponding author: Luis Irio (l.irio@campus.fct.unl.pt)

This work was supported in part by the Project CoSHARE under Grant LISBOA-01-0145-FEDER-0307095 - PTDC/EEI-TEL/30709/2017, in part by the Project UID/EEA/50008/2019, under Grant SFRH/BD/108525/2015, in part by the Fundo Europeu de Desenvolvimento Regional (FEDER), through Programa Operacional Regional LISBOA under Grant LISBOA2020, and in part by the National Funds, through Fundação para a Ciência e Tecnologia (FCT).

ABSTRACT This paper derives the distribution of the residual self-interference (SI) power in an analog post-mixer canceler adopted in a wireless in-band full-duplex communication system. We focus on the amount of uncanceled SI power due to SI channel estimation errors. Closed form expressions are provided for the distribution of the residual SI power when Rician and Rayleigh fading SI channels are considered. Moreover, the distribution of the residual SI power is derived for low and high channel gain dynamics, by considering the cases when the SI channel gain is time-invariant and time-variant. While for time-invariant channels the residual SI power is exponentially distributed, for time-variant channels the exponential distribution is not a valid assumption. Instead, the distribution of the residual SI power can be approximated by a product distribution. Several Monte Carlo simulation results show the influence of the channel dynamics on the distribution of the residual SI power. Finally, the accuracy of the theoretical approach is assessed through the comparison of numerical and simulated results, which confirm its effectiveness.

INDEX TERMS In-band full-duplex radio systems, residual self-interference power, stochastic modeling, performance analysis.

I. INTRODUCTION

Current wireless communication systems, including but not limited to cellular and local area networks, are half-duplex communication systems, meaning that the available resources are divided either in time domain or in frequency domain. Consequently, transmission and reception occur either at different times or in different frequency bands. Recently, a different approach has been investigated where the wireless terminals transmit and receive simultaneously over the same frequency band [1]–[3], which is known as In-Band Full Duplex (FDX) communications [4], [5].

By using FDX communications, the capacity of the communication link may be increased up to twice the amount of half-duplex communication systems [6]–[8]. However, to simultaneously transmit and receive, a terminal must separate its own transmission from the received signal, which is usually referred to as self-interference cancellation (SIC), posing several challenges at different levels, ranging from circuit design to signal processing.

The associate editor coordinating the review of this manuscript and approving it for publication was Khalil Afzal.

The success of FDX communications relies on the performance of SIC schemes. Since the transmitted signal may suffer different propagation effects, a terminal cannot simply cancel self-interference (SI) by subtracting its transmitted signal from the received one. Rather, digital-domain cancellation (DC) must be employed to account for the estimated effects of the propagation channel [9], [10]. But it is well known that DC is unable to completely suppress the SI [11]. Consequently, the SI is usually reduced before the DC through the adoption of an analog-domain cancellation (AC) technique [12], [13]. By using the two types of cancellation, the channel unaware AC technique suppresses a significant amount of direct-path SI, while the channel aware DC technique may suppress the remaining SI [14].

In this paper we characterize the distribution of the residual self-interference power in an analog post-mixer canceler, which represents the amount of uncanceled self-interference due to imperfect self-interference channel estimation and imperfections in the transmission chain [11]. Closed form expressions are derived for the distribution of the residual self-interference power when Rician and Rayleigh fading

self-interference channels are considered. The distribution of the residual self-interference power is also derived for low and high channel gain dynamics, by considering the cases when the self-interference channel gain is time-invariant and time-variant. Finally, we present different simulation results to show the influence of the channel dynamics on the distribution of the self-interference power. The accuracy of the proposed methodology is also evaluated for the limit case, when the frequency of the signal to transmit approaches the carrier frequency.

The rest of the paper is organized as follows. Next we review relevant research works related with the design and analysis of In-Band Full Duplex communication systems. Section II introduces the assumptions made regarding the system model. Section III describes the steps involved in the theoretical characterization of the residual SI power. The accuracy of the proposed methodology is evaluated in Section IV, where numerical results computed with the proposed model and Monte Carlo simulation results are compared. Finally, Section V concludes the paper by outlining its contribution.

Notations: In this work, $f_X(.)$ and $F_X(.)$ represent the probability density function (PDF) and the cumulative distribution function (CDF) of a random variable X, respectively. $\delta(.)$ denotes the Dirac's delta function. $\Gamma(.)$ represents the complete Gamma function. $K_v(.)$ denotes the modified Bessel function of the second kind with order v. $\mathcal{N}(\mu, \sigma)$ represents a Gaussian random variable with mean μ and variance σ. Gamma(k, θ) denotes a Gamma distribution with a shape parameter k and a scale parameter θ. Exp(λ) denotes an Exponential distribution with rate parameter λ and χ^2_1 represents a chi-squared distribution with 1 degree of freedom.

A. RELATED WORK

In FDX communications, the transmitter's (TX) signal must be reduced to an acceptable level at the receiver (RX) located in the same node. Any residual SI will increase the RX noise floor, thus reducing the capacity of the RX channel. FDX communications' performance is limited by the amount of SI suppression, which may be achieved by two different methods:

- Antenna Isolation (AI) [15], [16], to prevent the RF-signal generated by the local TX from leaking onto the RX;
- Self-interference Cancellation (SIC) [9], [10], [13], to subtract any remaining SI from the RX path using knowledge of the TX signal and channel estimation.

AI is fundamentally limited by the physical separation of the antennas [16]. The SIC performance depends on the accuracy with which the transmitted signal can be copied, modified and subtracted. The signal to be subtracted is usually a modified copy of the transmitted one, obtained by a simulated channel path between the points where signals are sampled and subtracted. Three different active SIC architectures are reported in the literature:

- Analog-domain cancellation [17], [18];
- Digital-domain cancellation [4], [9], [19];
- Mixed-signal cancellation (MXC) [20]–[22].

AC schemes can provide up to 40-50 dB cancellation [18], exhibiting higher performance than DC. This is explained by the fact that the cancellation signal includes all TX impairments, and it relaxes requirements further downstream. However, it requires processing the cancellation signal in the analog RF domain, increasing hardware costs and complexity. AC cancellation can be done either at the analog baseband or at the carrier radio-frequency (RF). The cancelling signal may be generated by processing the SI signal prior to the upconversion stage (pre-mixer cancellers), or after the SI signal being upconverted (post-mixer cancellers). In both cases, the performance is limited by the phase noise of the oscillators used in the up/down conversion [20], [23]. AC presents several challenges, which may include the non-linear effects of power amplifiers [11], [24], the In-phase/Quadrature (IQ) imbalance [24], [25], and the phase noise of both transmitter and receiver [23], [26], [27].

In DC schemes the signals are processed in the digital domain, making use of all digital benefits, including the SI wireless channel awareness, through adequate channel estimation techniques. However, DC cannot remove the SI in the analog RX chain, being unable to prevent the analog circuitry to block the reception due to nonlinear distortion or the ADCs' quantization error [28]. It is well known that DC is unable to completely suppress the SI, mainly because the dynamic range of the analog-to-digital converters (ADC) limits the amount of suppressed SI, due to the limited effective number of bits (ENOB) [11], [29]. Commercial ADCs have improved significantly in sampling frequency but only marginally in ENOB. DC can provide up to 30-35 dB cancellation in practice [30], being limited by a noisy estimate of the SI channel and noisy components of the self-interferer that cannot be cancelled [31], [32].

In MXC schemes, both AC and DC are considered. The digital TX signal is processed and converted to analog radio-frequency (RF), where subtraction occurs [20], [21], and it is processed after the AC [20], [22]. This requires a dedicated additional upconverter, which limits the cancellation of current MXC schemes to 35 dB [20]. To achieve overall SI suppression close to 100 dB above the noise floor, both AC and DC must be used in a MXC scheme.

The residual SI is mainly due to estimation errors occurring during the time domain cancellation [28], and has been addressed in various works in the literature [11], [33]–[39]. [11] has identified the quantization-noise, the phase-noise in the local oscillator, and the channel estimation error, as being the main causes of incomplete self-interference cancellation in different FDX schemes. Reference [33] analyzed the impact of the phase-noise on the distribution of the residual SI power, showing that the phase-noise is almost negligible when the oscillators' phase-noise is close to the minimum achievable phase noise of RC oscillators [40]. However, we highlight that the

conclusions in [33] are only based on simulations without any theoretical understanding. Reference [34] has analyzed non-linear distortion effects occurring in the transmitter power amplifier and also due to the quantization noise of the ADCs at the receiver chain. The uncertainty associated with the residual self-interference channel was studied in [35], which has proposed a block training scheme to estimate both communication and residual SI channels in a two-way relaying communication system. The residual SI channel was also studied in [36], showing that the channel can be modeled as a linear combination of the original signal and its derivatives. The authors adopt a Taylor series approximation to model the channel with only two parameters, and a new SI cancellation scheme based on the proposed channel model is also described. Reference [37] investigates the detrimental effects of phase noise and in-phase/quadrature imbalance on full-duplex OFDM transceivers, showing that more sophisticated digital-domain SI cancellation techniques are needed to avoid severe performance degradation. Reference [37] derives a closed-form expression for the average residual self-interference power and describes its functional dependence on the parameters of the radio-frequency impairments. The residual SI is also characterized in [38] for a multi-user multiple-input multiple-output (MIMO) setup considering FDX multi-antenna nodes and assuming the availability of perfect channel state information. The authors show that for the MIMO scenario the residual SI can be approximated by a Gamma distribution assuming time-invariant channels. Reference [39] investigated if the residual SI power can be accurately approximated by known distributions. The paper shows that Weibull, Gamma and Exponential distributions fail to approximate the residual SI power in an accurate way. This observation was only based on Monte Carlo simulation results, from which the parameters of the known distributions were obtained using a fitting tool based on the Maximum Likelihood Estimation method. The results in [39] have motivated us to derive the distribution of the residual SI power in a theoretical way, which is the main topic addressed in this paper.

B. CONTRIBUTIONS

Motivated by the importance of the analog SI's characterization in the joint cancellation process, this work derives a theoretical analysis of the residual SI power, i.e., the amount of uncanceled self-interference due to channel estimation errors at the analog cancellation process. The proposed analysis neglects the nonlinear effects due to RF impairments (e.g. ADCs and power amplifier impairments), although the impact of the phase noise is analyzed through Monte Carlo simulation results. We believe that our work is a first step to derive more complex models, as nonlinear effects can be modeled as a linear combination of multiple input signals [36].

To the best of the authors' knowledge, this is the first work deriving the distribution of the residual self-interference power in an analog post-mixer canceler scheme. The results and the insights presented in this work are new and can definitely be used as a benchmark for future studies. Our contributions are as follows:

- We derive closed form expressions for the distribution of the residual SI power when Rician and Rayleigh fading self-interference channels are considered;
- The impact of the fading channel is evaluated on the distribution of the residual SI power and the results achieved confirm that the type of fading channel strongly impacts the distribution of the residual SI power;
- The distribution of the residual SI power is derived for low and high channel gain dynamics, showing that the channel dynamics strongly influences the distribution of the self-interference power;
- Numerical results computed with the proposed model are compared with Monte Carlo simulation results to evaluate the accuracy of the theoretical analysis for both SI channel's gain and phase estimation errors;
- The accuracy of the theoretical analysis is also assessed for the limit case when the frequency of the input signal to be transmitted is close to the carrier frequency. In this way we identify the dynamic region where the proposed approach achieves high accuracy;
- The impact of the phase noise is evaluated through Monte Carlo simulation results for different values of phase noise variance.

The need of analog and digital-domain cancellation requires a precise characterization of the amount of interference not canceled in the analog-domain. The knowledge of the residual SI due to the AC is crucial to design efficient SI estimation methods to be used in the digital-domain. By doing so, the efficiency of the joint AC and DC schemes may be improved.

II. SYSTEM MODEL

In this work we consider a full-duplex scheme adopting an active analog canceler that reduces the self-interference at the carrier frequency. The active analog canceler actively reduces the self-interference by injecting a canceling signal into the received signal. A post-mixer canceler is assumed, because the canceling signal is generated by processing the self-interference signal after the upconversion stage [23]. The block diagram of the system model is shown in Fig. 1.

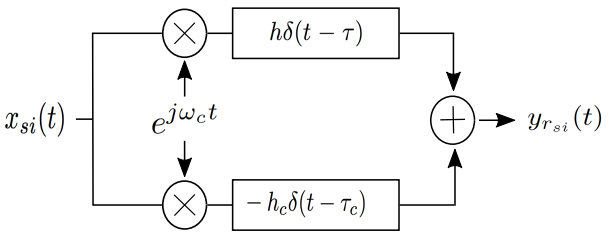

FIGURE 1. Block diagram representation of the post-mixer canceller.

The self-interference signal $x_{si}(t)$ is up-converted to the frequency $\omega_c = 2\pi f_c$ and transmitted over the full-duplex channel characterized by the gain h and the delay τ. In this

work we consider that the active analog canceler estimates the channel's gain and delay in order to reduce the residual self-interference $y_{r_{si}}(t)$.

The residual self-interference, $y_{r_{si}}(t)$, is represented as follows

$$y_{r_{si}}(t) = x_{si}(t)e^{j\omega_c t} * \mathbf{h}_{si}(t) - x_{si}(t)e^{j\omega_c t} * \hat{\mathbf{h}}_{si}(t), \quad (1)$$

where $x_{si}(t)$ is the SI signal, $\mathbf{h}_{si}(t)$ is the impulse response of the SI channel, $\hat{\mathbf{h}}_{si}(t)$ represents the estimate of the SI channel, ω_c is the angular frequency and $*$ represents the convolution operation. The SI channel considered in our work is a single-tap delay channel, i.e., $\mathbf{h}_{si}(t) = h\delta(t-\tau)$. Similarly, the estimate of the SI channel is denoted by $\hat{\mathbf{h}}_{si}(t) = h_c\delta(t-\tau_c)$, where h_c and τ_c are the estimated SI channel's gain and delay, respectively.

We assume that the SI signal, $x_{si}(t)$, is a circularly-symmetric complex signal, representing the case when Orthogonal Frequency-Division Multiplexing with a high number of sub-carriers is adopted [41]. Departing from the residual SI in (1), it can be rewritten as

$$y_{r_{si}}(t) = h\, x_{si}(t-\tau)e^{j(\omega_c(t-\tau))} - h_c\, x_{si}(t-\tau_c)e^{j(\omega_c(t-\tau_c))}. \quad (2)$$

In what follows we consider that the channel gain is complex, $h = h_r + jh_j$, and the estimate of the channel's gain is given by $h_c = \epsilon h$, where $(1-\epsilon)$ is the channel's gain estimation error. Channel's phase estimation error is represented by $\psi = \omega_c(\tau - \tau_c)$. We also consider that the SI signal $x_{si}(t)$ is a random signal, whose value for a specific sample k is represented by a pair of two random variables (RVs) $\{X_r, X_j\}$, i.e. for a specific sample k we represent $x_{si}(k\Delta_T) = X_r + jX_j$, where Δ_T represents the sample period. If the sample period is low, i.e. $\Delta_T << 2\pi/\omega_c$, and the value of the RVs $X_r + jX_j$ remain constant for several samples, we may assume that $\Pr[x_{si}(t-\tau) - x_{si}(t-\tau_c) = 0]$ is high, since the SI signal $x_{si}(k\Delta_T)$ may remain constant for a consecutive number of samples[1]. After a few algebraic manipulations, the residual SI can be represented by its real and imaginary parts, $\Re\{y_{r_{si}}\}$ and $\Im\{y_{r_{si}}\}$, respectively, defined by

$$\Re\{y_{r_{si}}\} = \alpha X_r + \beta X_j, \quad (3)$$
$$\Im\{y_{r_{si}}\} = -\beta X_r + \alpha X_j. \quad (4)$$

(2) can be used in the system of 2 equations formed by (3) and (4), to obtain α and β, which are respectively given by

$$\alpha = h_r\cos(\omega_c(t-\tau)) - \epsilon h_r\cos(\omega_c(t-\tau_c)) - h_j\sin(\omega_c(t-\tau)) + \epsilon h_j\sin(\omega_c(t-\tau_c)), \quad (5)$$

and

$$\beta = -h_j\cos(\omega_c(t-\tau)) + \epsilon h_j\cos(\omega_c(t-\tau_c)) - h_r\sin(\omega_c(t-\tau)) + \epsilon h_r\sin(\omega_c(t-\tau_c)). \quad (6)$$

Using (3) and (4), the residual SI power after cancellation can be written as follows

$$P_{y_{r_{si}}} = \left(X_r^2 + X_j^2\right)\left(\alpha^2 + \beta^2\right), \quad (7)$$

which represents the amount of interference power received due to inability to cancel the SI.

III. CHARACTERIZATION OF THE RESIDUAL SI

In this section we describe the steps required to derive the distribution of the residual SI. Motivated by the fact that the channel may have different dynamics, we consider two different cases:

- *Low channel dynamics* - in this scenario the channel gain is almost time-invariant, and consequently h and h_c can be considered constants;
- *High channel dynamics* - in this scenario the channel gain is clearly time-variant, and consequently h and h_c are assumed to be RVs.

A. HIGH CHANNEL DYNAMICS

By considering the case when the channel gain is time-varying and $x_{si}(t)$ is a circularly-symmetric complex signal, i.e., $X_r \sim \mathcal{N}(0, \sigma_x^2)$ and $X_j \sim \mathcal{N}(0, \sigma_x^2)$, Theorem 1 gives the distribution of the residual SI power when we consider a SI Rician fading channel, i.e., the time-varying variables h_r and h_j are realizations of the random variables $H_r \sim \mathcal{N}(\mu_h\cos(\vartheta), \sigma_h^2)$ and $H_j \sim \mathcal{N}(\mu_h\sin(\vartheta), \sigma_h^2)$, respectively. On other hand, Theorem 2 characterizes the distribution of the residual SI power when a SI Rayleigh fading channel is considered, where $H_r \sim \mathcal{N}(0, \sigma_h^2)$ and $H_j \sim \mathcal{N}(0, \sigma_h^2)$.

Theorem 1: When the self-interference channel gain is distributed according to a Rice[2] distribution with non-centrality parameter μ_h and scale parameter σ_h, the probability density function of the self-interference power follows a product distribution given by

$$f_{P_{y_{r_{si}}}}(z) = \frac{2^{(1/2-k_h/2)}\sigma_x^{(-k_h-1)}\lambda_A^{-k_h}}{\Gamma(k_h)} \times(\lambda_A/z)^{\frac{k_h-1}{2}} z^{k_h-1}K_{(k_h-1)}\left(\sqrt{\frac{2z}{\sigma_x^2\lambda_A}}\right) \quad (8)$$

where $K_{(k_h-1)}(.)$ is the modified Bessel function of the second kind ($(K_n(x))$ for $n = k_h - 1$), and λ_A, k_h and θ_h are given by

$$\lambda_A = \theta_h\left[1 + \epsilon^2 - 2\epsilon\cos\left(\omega_c(\tau - \tau_c)\right)\right], \quad (9)$$

[1] While this approximation may be quite simplistic at this stage, the validation results presented in Section IV show that it does not compromise the accuracy of the proposed modeling methodology. This is mainly because $X_r + jX_j$ take the same value for a consecutive number of samples, since the carrier frequency (and consequently the sampling frequency, Δ_T) is higher than any frequency component of the input signal x_{si}.

[2] The Rice distribution was assumed because the SI channel is formed between two antennas that are close to each other, in which there is a strong Line-of-Sight component. Since the Rician fading model assumes that the received signal is the result of a dominant component (the Line-of-Sight component), the SI channel is usually modeled by a Rician fading channel [28], [38], [42].

$$k_h = \frac{(\mu_h^2 + 2\sigma_h^2)^2}{4\sigma_h^2(\mu_h^2 + \sigma_h^2)}, \tag{10}$$

$$\theta_h = \frac{4\sigma_h^2(\mu_h^2 + \sigma_h^2)}{\mu_h^2 + 2\sigma_h^2}. \tag{11}$$

Proof: Departing from (7), and assuming that $X_r \sim \mathcal{N}(0, \sigma_x^2)$ and $X_j \sim \mathcal{N}(0, \sigma_x^2)$, then X_r^2 and X_j^2 are distributed according to a chi-squared distribution with 1 degree of freedom, denoted by χ_1^2. X_r and X_j may be written as follows

$$X_r^2 \sim \sigma_x^2 {\chi_1}^2, \tag{12}$$

$$X_j^2 \sim \sigma_x^2 {\chi_1}^2. \tag{13}$$

By definition, if $Y \sim \chi_k^2$ and $c > 0$, then $cY \sim \text{Gamma}(k/2, 2\,c)$. Consequently,

$$X_r^2 \sim \text{Gamma}(1/2, 2\sigma_x^2), \tag{14}$$

and

$$X_j^2 \sim \text{Gamma}(1/2, 2\sigma_x^2). \tag{15}$$

Knowing that the sum of two gamma RVs with different shape parameters is given by $\text{Gamma}(k_1, \theta) + \text{Gamma}(k_2, \theta) \sim \text{Gamma}(k_1 + k_2, \theta)$, we have

$$X_r^2 + X_j^2 \sim \text{Gamma}(1, 2\sigma_x^2). \tag{16}$$

Departing again from (7), the term $\left(\alpha^2 + \beta^2\right)$ is a random variable because h_r and h_j are time-varying variables representing realizations of the random variables H_r and H_j, respectively. After a few algebraic manipulations, and replacing h_r and h_j by the random variables H_r and H_h, respectively, we obtain

$$\alpha^2 + \beta^2 = (H_j^2 + H_r^2)\left[1 + \epsilon^2 - 2\epsilon\cos\left(\omega_c(\tau - \tau_c)\right)\right]. \tag{17}$$

The Rician fading channel is described by parameters K and Ω, where K is the ratio between the power of Line-of-Sight (LOS) path and the power in the other reflected paths, and Ω is the total power from both paths. The signal envelope is Rician distributed with parameters $\mu_h = \sqrt{\frac{K\Omega}{1+K}}$ and $\sigma_h = \sqrt{\frac{\Omega}{2(1+K)}}$. K can also be expressed in decibels by the variable $K_{dB} = 10\log_{10}(K)$.

Defining ${H_p}' = (1/\sigma_h^2)(H_j^2 + H_r^2)$, ${H_p}'$ follows a non-central Chi-square distribution with two degrees of freedom, and non centrality parameter $\frac{{\mu_h}^2}{{\sigma_h}^2}$.

Applying the method of moments to provide a Gamma approximation for the distribution of ${H_p}'$, we obtain the following shape and scale parameters,

$${k_h}' = \frac{(\mu_h^2 + 2\sigma_h^2)^2}{4\sigma_h^2(\mu_h^2 + \sigma_h^2)}, \tag{18}$$

$${\theta_h}' = \frac{4(\mu_h^2 + \sigma_h^2)}{\mu_h^2 + 2\sigma_h^2}. \tag{19}$$

Since we have considered ${H_p}'$ instead of $H_j^2 + H_r^2$, the distribution that represents the residual SI channel power gain is approximatted by

$$H_j^2 + H_r^2 \sim \text{Gamma}(k_h, \theta_h), \tag{20}$$

following the same steps to obtain (16), where $k_h = {k_h}'$ and $\theta_h = \sigma_h^2{\theta_h}'$.

Because $\left[1 + \epsilon^2 - 2\epsilon\cos\left(\omega_c(\tau - \tau_c)\right)\right]$ is a constant, and knowing that when $Y \sim \text{Gamma}(k, \theta)$ and $c > 0$, $cY \sim \text{Gamma}(k, c\theta)$, then

$$(H_j^2 + H_r^2)\left[1+\epsilon^2 - 2\epsilon\cos\left(\omega_c(\tau - \tau_c)\right)\right] \sim$$

$$\sim \text{Gamma}\left(k_k, \theta_h\left[1+\epsilon^2 - 2\epsilon\cos\left(\omega_c(\tau - \tau_c)\right)\right]\right). \tag{21}$$

In (7) the term $(\alpha^2 + \beta^2)$ only depends on the random variables H_r and H_j, and consequently is independent of the term $(X_r^2 + X_j^2)$. Because in (7) we have the product of the two terms, the probability density function of $P_{y_{rsi}}$ is given by the classical product probability density function expressed as follows

$$f_{P_{y_{rsi}}}(z) = \int_{-\infty}^{\infty} f_{X_r^2+X_j^2}(x) f_{\alpha^2+\beta^2}(z/x)\frac{1}{|x|}\,dx. \tag{22}$$

Replacing $f_{X_r^2+X_j^2}(x)$ and $f_{\alpha^2+\beta^2}(z/x)$ in (22) by (16) and (21), respectively, we obtain (23). Solving the integral in (23), shown at the bottom of this page, we finally obtain

$$f_{P_{y_{rsi}}}(z) = \frac{2^{(1/2-k_h/2)}\sigma_x^{(-k_h-1)}\lambda_A^{-k_h}}{\Gamma(k_h)} \times(\lambda_A/z)^{\frac{k_h-1}{2}} z^{k_h-1} K_{(k_h-1)}\left(\sqrt{\frac{2z}{\sigma_x^2\lambda_A}}\right). \tag{24}$$

The CDF of the residual SI power is given by

$$F_{P_{y_{rsi}}}(z) = 1 - \left(\frac{2^{(1-k_h/2)}(\lambda_A z)^{k_h/2} \quad K_{k_h}\left(\sqrt{\frac{2z}{\sigma_x^2\lambda_A}}\right)}{(\sigma_x\lambda_A)^{k_h}\Gamma(k_h)}\right), \tag{25}$$

$$f_{P_{y_{rsi}}}(z) = \int_{-\infty}^{\infty} \frac{\left([1 + \epsilon^2 - 2\epsilon\cos(\omega_c(\tau - \tau_c))]\theta_h\right)^{-k_h}}{2\sigma_x^2\Gamma(k_h)|x|}\left(\frac{z}{x}\right)^{k_h-1} e^{-\frac{x}{2\sigma_x^2} - \frac{z}{\theta_h x[1 + \epsilon^2 - 2\epsilon\cos(\omega_c(\tau - \tau_c))]}}\,dx. \tag{23}$$

where $K_{k_h}(.)$ is the modified Bessel function of the second kind (($K_n(x)$) for $n = k_h$). ■

Theorem 2: When the self-interference channel gain is distributed according to a Rayleigh distribution with scale parameter σ_h, the probability density function of the self-interference power follows a product distribution given by

$$f_{P_{y_{r_{si}}}}(z) = \frac{K_0\left(\sqrt{\frac{2z}{\sigma_x^2\lambda_B}}\right)}{\sigma_x^2\lambda_B}, \tag{26}$$

where $K_0(.)$ is the modified Bessel function of the second kind, and λ_B is given by

$$\lambda_B = 2\sigma_h^2\left[1+\epsilon^2-2\epsilon\cos\left(\omega_c(\tau-\tau_c)\right)\right]. \tag{27}$$

Proof: Assuming again that $X_r \sim \mathcal{N}(0,\sigma_x^2)$ and $X_j \sim \mathcal{N}(0,\sigma_x^2)$, the term $X_r^2+X_j^2$ has the same distribution represented in (16).

In this case, when $H_r \sim \mathcal{N}(0,\sigma_h^2)$ and $H_j \sim \mathcal{N}(0,\sigma_h^2)$, the random variable that represents $H_j^2+H_r^2$ is given by

$$H_j^2+H_r^2 \sim \text{Gamma}(1, 2\sigma_h^2), \tag{28}$$

following the same steps to obtain (16). As the term $\left[1+\epsilon^2-2\epsilon\cos\left(\omega_c(\tau-\tau_c)\right)\right]$ is a constant, then

$$(H_j^2+H_r^2)\left[1+\epsilon^2-2\epsilon\cos\left(\omega_c(\tau-\tau_c)\right)\right] \sim$$
$$\sim \text{Gamma}\left(1, 2\sigma_h^2\left[1+\epsilon^2-2\epsilon\cos\left(\omega_c(\tau-\tau_c)\right)\right]\right). \tag{29}$$

Replacing $f_{X_r^2+X_j^2}(x)$ and $f_{\alpha^2+\beta^2}(z/x)$ in (22) by (16) and (29), respectively, we obtain (30). Solving the integral in (30), shown at the bottom of this page, we finally obtain

$$f_{P_{y_{r_{si}}}}(z) = \frac{K_0\left(\sqrt{\frac{2z}{\sigma_x^2\lambda_B}}\right)}{\sigma_x^2\lambda_B}, \tag{31}$$

where $K_0(.)$ is the modified Bessel function of the second kind (($K_n(x)$) for $n=0$) and $\lambda_B = 2\sigma_h^2\left[1+\epsilon^2-2\epsilon\cos\left(\omega_c(\tau-\tau_c)\right)\right]$. The CDF of the residual SI power is given by

$$F_{P_{y_{r_{si}}}}(z) = 1-\left(\frac{\sqrt{2\lambda_B z}\quad K_1\left(\sqrt{\frac{2z}{\sigma_x^2\lambda_B}}\right)}{\sigma_x\lambda_B}\right), \tag{32}$$

where $K_1(.)$ is the modified Bessel function of the second kind (($K_n(x)$) for $n=1$). ■

B. LOW CHANNEL DYNAMICS

By considering the case when the channel gain is constant and $x_{si}(t)$ is a circularly-symmetric complex signal, i.e., $X_r \sim \mathcal{N}(0,\sigma_x^2)$ and $X_j \sim \mathcal{N}(0,\sigma_x^2)$, Theorem 3 shows that the distribution of the residual SI power follows an exponential distribution with rate parameter λ_C.

Theorem 3: When the channel gain is constant the self-interference power is exponentially distributed, i.e.

$$f_{P_{y_{r_{si}}}}(z) = \frac{e^{\frac{-z}{\lambda_C}}}{\lambda_C}, \tag{33}$$

with rate parameter

$$\lambda_C = \frac{1}{2\sigma_x^2\left(h_r^2+h_j^2\right)\left[1+\epsilon^2-2\epsilon\cos\left(\omega_c(\tau-\tau_c)\right)\right]}. \tag{34}$$

Proof: Once again we assume that $X_r \sim \mathcal{N}(0,\sigma_x^2)$ and $X_j \sim \mathcal{N}(0,\sigma_x^2)$, then the term $X_r^2+X_j^2$ has the same distribution represented in (16).

Contrarily to the case assumed in the Subsection III-A, when h and h_c are considered constant, $h_r \in \mathbb{R}$ and $h_j \in \mathbb{R}$, then $\left(\alpha^2+\beta^2\right) \in \mathbb{R}$, and $\left(\alpha^2+\beta^2\right) > 0$. Departing from (7), using (16), and knowing that when $Y \sim \text{Gamma}(k,\theta)$ and $c>0$, $cY \sim \text{Gamma}(k, c\theta)$, we obtain

$$P_{y_{r_{si}}} \sim \text{Gamma}\left(1, 2\sigma_x^2\left(\alpha^2+\beta^2\right)\right). \tag{35}$$

Because $\text{Gamma}(1,\lambda^{-1}) \sim \text{Exp}(\lambda)$, $P_{y_{r_{si}}}$ can be rewritten as follows

$$P_{y_{r_{si}}} \sim \text{Exp}\left((2\sigma_x^2\left(\alpha^2+\beta^2\right))^{-1}\right). \tag{36}$$

Using (5) and (6), (36) is finally rewritten as follows

$$P_{y_{r_{si}}} \sim \text{Exp}\left(\frac{1}{2\sigma_x^2\left(h_r^2+h_j^2\right)\left[1+\epsilon^2-2\epsilon\cos\left(\omega_c(\tau-\tau_c)\right)\right]}\right).$$

The Cumulative Distribution Function (CDF) of the residual SI power is given by

$$F_{P_{y_{r_{si}}}}(z) = 1-e^{\frac{-z}{\lambda_C}}. \tag{37}$$

■

$$f_{P_{y_{r_{si}}}}(z) = \int_{-\infty}^{\infty} \frac{1}{4\sigma_x^2\sigma_h^2\Gamma(1)^2[1+\epsilon^2-2\epsilon\cos(\omega_c(\tau-\tau_c))]|x|} e^{-\frac{x}{2\sigma_x^2}-\frac{z}{2\sigma_h^2 x[1+\epsilon^2-2\epsilon\cos(\omega_c(\tau-\tau_c))]}}\,dx. \tag{30}$$

IV. VALIDATION AND RESULTS

This section evaluates the accuracy of the derivation proposed in Section III. The evaluation methodology is presented in Subsection IV-A and the accuracy of the derivation is discussed in Subsection IV-B.

A. EVALUATION METHODOLOGY

The accuracy of the residual SI power distribution is evaluated through the comparison of Monte Carlo simulations with numerical results, obtained from the derivation presented in Section III. The comparison includes different channel conditions and SI cancellation errors.

Regarding the simulations, we have simulated the post-mixer canceller presented in Fig.1. The simulation results were obtained using the Monte Carlo method during 200 μs of simulation time (72×10^6 samples were collected during each simulation). The up-conversion frequency was parametrized to $\omega_c = 2\pi \times 10^9$ rad/s, i.e., the FDX communication system is operating at a carrier frequency of 1 GHz (equivalent to a period $T_c = 1$ ns). In the simulations we adopted a sample period $\Delta_T = T_c/360$. The values of X_r and X_j were sampled from Normal distributions, $\mathcal{N}(0, \sigma_x^2)$, each $4T_c$ (with $\sigma_x^2 = \frac{1}{2}$). H_r and H_j were sampled from normal distributions ($H_r \sim \mathcal{N}(\mu_h \cos(\vartheta), \sigma_h^2)$, $H_j \sim \mathcal{N}(\mu_h \sin(\vartheta), \sigma_h^2)$ for Rician fading, and $H_r \sim \mathcal{N}(0, \sigma_h^2)$, $H_j \sim \mathcal{N}(0, \sigma_h^2)$ for Rayleigh fading). For time-variant channels, H_r and H_j were sampled each $40T_c$. Differently, for time-invariant channels, h_r and h_j were maintained constant during the simulation ($h_r^2 = h_j^2 = 1/2$ was assumed). We highlight that we have considered an average unitary channel gain in all fading channels, to guarantee a fair comparison. In the simulations, the residual SI was determined for each simulation sample collected each Δ_T, by computing (2). The residual SI power was also computed for each sample using (7). The parameters adopted in the simulations are presented in Table 1.

TABLE 1. Parameters adopted in the simulations.

f_c	1 GHz	ω_c	$2\pi \times 10^9$ rad/s
σ_x^2	$1/2$	ψ	$\{\pi/18, \pi/9, \pi/6\}$
T_c	1 ns	ϵ	$\{0.95, 0.90, 0.80\}$
Δ_T	$1/360$ ns	Simulation time	200 μs
ϑ	$\pi/4$	K_{dB}	$\{-10, 0, 3, 10\}$
Ω	1		

The numerical results were obtained computing (24) and (25) for time-variant Rician channels, (32) for time-variant Rayleigh channels, and (37) for time-invariant channels, respectively. From (24), (25), (32), and (37), we observe that the computation of the distribution of the residual SI power only depends on the statistics of the SI signal (X_r, X_j), the statistics of the SI channel (H_r, H_j), the channel's gain estimation accuracy (ϵ), and channel's phase estimation error (ψ).

B. ACCURACY ASSESSMENT

First, we evaluate the distribution of the residual SI power for different values of channel's gain estimation accuracy (ϵ) and considering perfect estimation of the channel's delay ($\tau = \tau_c$). Time-invariant and Rayleigh time-variant channels are compared. Numerical results are compared with simulation results in Fig. 2. In the figure the "inv" curve represents the results obtained with the time-invariant channel. The "var - Rayleigh" curve represents the results obtained with the time-variant channel, when a Rayleigh fading self-interference channel is considered, with $\sigma_h^2 = \frac{1}{2}$. The CDF is plotted for different channel's gain estimation accuracy values ($\epsilon = [0.95, 0.90, 0.80]$). The "Simulation" curves represent the results obtained through Monte Carlo simulatiom. The "Model" curves were obtained with the computation of (37) and (32) for time-invariant and time-variant Rayleigh channels, respectively.

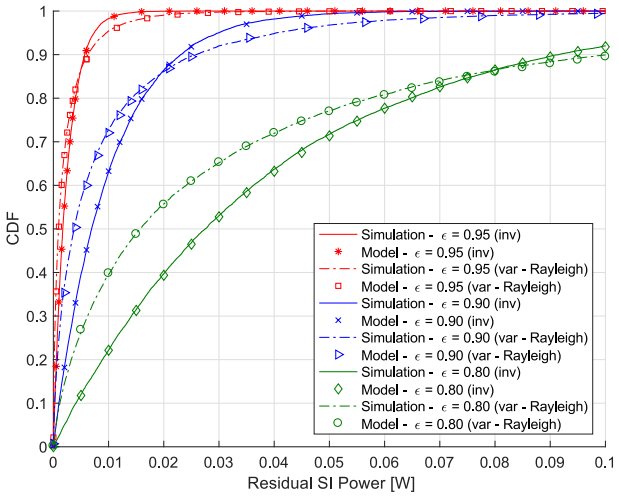

FIGURE 2. Residual SI Power for different values of ϵ (Rayleigh fading channel: $\sigma_h^2 = \frac{1}{2}$; Time-invariant channel: $h_r{}^2 = h_j{}^2 = 1/2$).

As can be seen, the numerical results computed with the proposed model are close to the results obtained through simulation. This is observed for the different levels channel's gain estimation accuracy and for the time-variant and invariant channels. As a general trend, it is observed that the SI power increases with the channel's gain estimation error ($1 - \epsilon$), as expected. Moreover, Fig. 2 shows that the probability of observing higher values of residual SI power increases when the time-variant channels are considered, because of its higher dynamics.

Next, we evaluate the distribution of the residual SI power for perfect estimation of the channel's gain ($\epsilon = 1$) and considering imperfect estimation of the channel's delay. Fig. 3 plots numerical and simulation results of the distribution of the residual SI power, adopting different phase estimation errors ($\psi = \omega_c(\tau - \tau_c) = [\pi/18, \pi/9, \pi/6]$). The results were obtained for a time-invariant channel, a time-variant Rayleigh channel, and a time-variant Rician channel. In this case the numerical results in the "Model" curves were

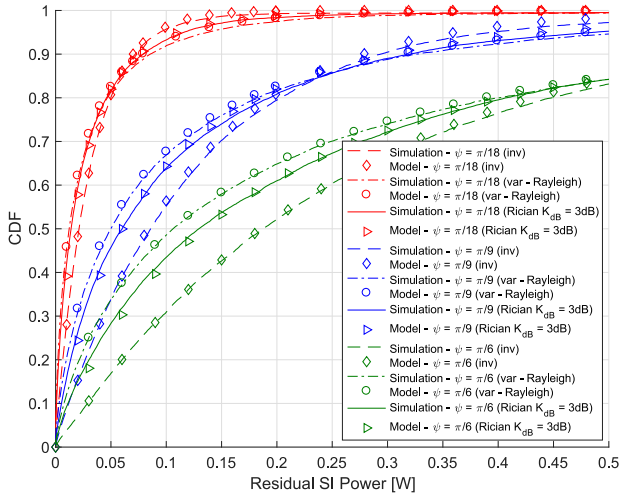

FIGURE 3. Residual SI Power for different values of ψ (Rayleigh fading: $\sigma_h^2 = \frac{1}{2}$; Rician fading: $K_{dB} = 3$ dB, $\mu_h = 0.8162$, $\sigma_h = 0.4086$).

computed with (25) and (32), for Rician fading and Rayleigh fading, respectively. Once again, the numerical results are close to the results obtained through simulation. As can be seen, the phase estimation error significantly impacts on the distribution of the residual SI power and the average residual SI power increases with the phase estimation error. Moreover, the different types of the fading channel lead to different distributions of the residual SI power (for the same value of phase estimation error).

To evaluate the impact of parameter K_{dB} on the distribution of the residual SI power, we next consider different parameterizations of the Rician fading channel, i.e., $K_{dB} = [-10, 0, 10]$ dB, for a single value of phase estimation error ($\psi = \pi/18$) and considering perfect estimation of the channel's gain ($\epsilon = 1$). Simulation and numerical results are presented in Fig. 4, which confirm the accuracy of the proposed methodology for both PDF and CDF (numerically computed from (24) and (25), respectively). From the results in the figure, we conclude that the average residual SI power increases with the ratio between the power of the LOS path and the power of the other reflected paths.

In Section 2 we have assumed that the input signal $X_r + jX_j$ may take the same value for a consecutive number of samples, since the carrier frequency (and consequently the sampling frequency) is higher than any frequency component of the input signal x_{si}. To assess the impact of such assumption we have performed different simulations considering that X_r and X_j are sampled from a Normal distribution at submultiples of the carrier frequency (f_c). Fig. 5 compares the residual SI power obtained with the simulation results when X_r and X_j remain constant during one, two, three, and four carrier periods (curves "Simulation - 1 T_c", "Simulation - 2 T_c", "Simulation - 3 T_c", and "Simulation - 4 T_c", respectively). As can be seen the accuracy of the proposed model increases as X_r and X_j remain with the same value for a longer period of time. The results show that the numerical results (represented

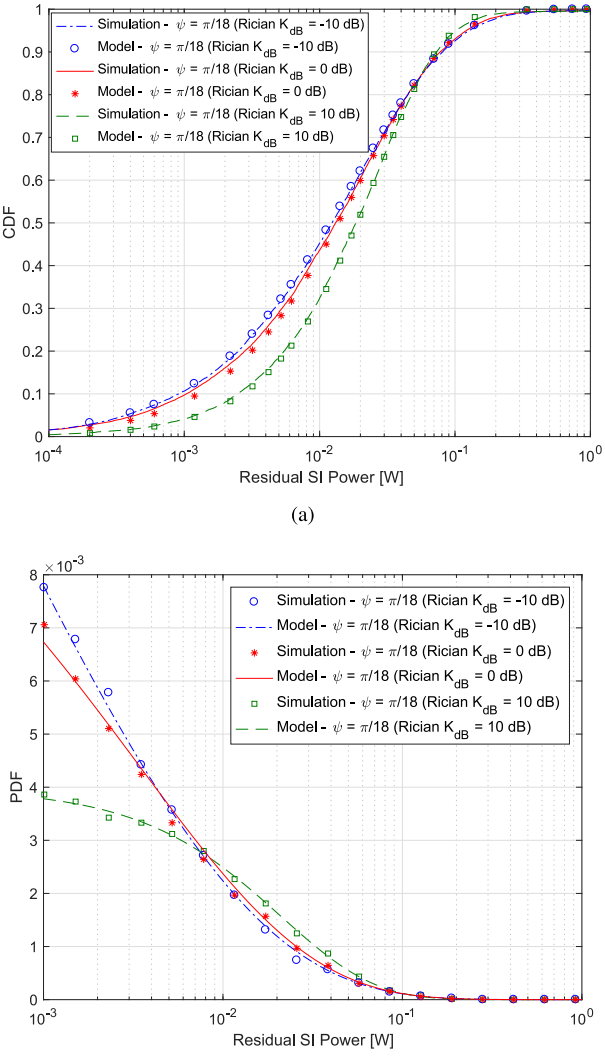

FIGURE 4. Residual SI Power for different values of K_{dB} (Rician fading: {K_{dB} = -10 dB; $\mu_h = 0.3015$; $\sigma_h = 0.6742$}, {$K_{dB} = 0$ dB; $\mu_h = 0.7071$; $\sigma_h = 0.5000$}, {$K_{dB} = 10$ dB; $\mu_h = 0.9535$; $\sigma_h = 0.2132$}).

by the curve "Model") are close to the simulated results, when X_r and X_j remain constant for approximately 4 carrier periods, which is a valid assumption from the practical viewpoint. The results in Fig. 5 confirm the accuracy of the proposed model, even when x_{si} exhibits high temporal dynamics.

Next we analyze the impact of the oscillator's phase-noise ($\phi(t)$) on the residual SI power. We consider a typical phase-noise value for a low power low area oscillator, built in a standard 130 nm CMOS technology, operating at 1 GHz [43], which may typically exhibit a phase-noise of approximately -100 dBc/Hz @ 1 MHz frequency offset. To determine the properties of the Gaussian distribution that represents the phase-noise, the oscillator phase-noise was simulated using the Matlab software package. The phase-noise distribution obtained from the data simulated with the phase-noise Simulink block was caracterized by

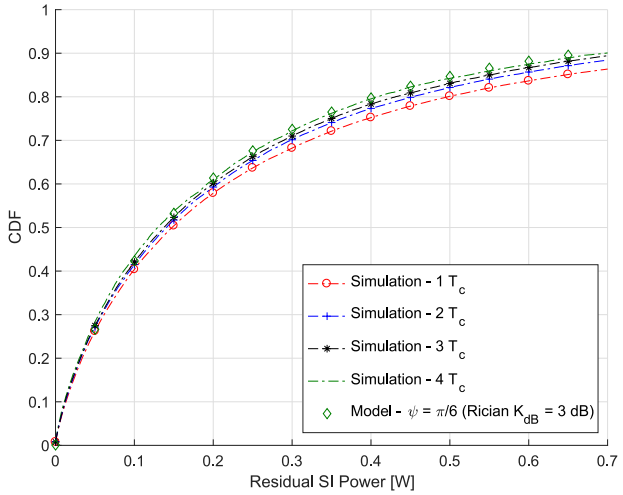

FIGURE 5. Residual SI Power for different sampling periods of $X_r + jX_j$ (Rician fading: $K_{dB} = 3$ dB, $\mu_h = 0.8162$, $\sigma_h = 0.4086$; $\psi = \pi/6$).

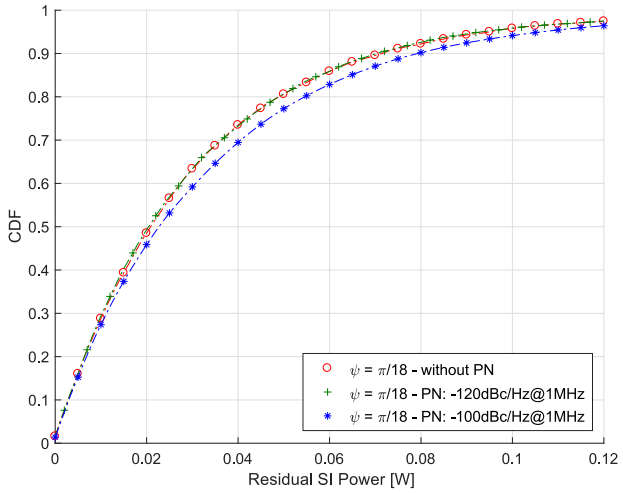

FIGURE 6. Residual SI Power for different values of phase-noise (Time-invariant channel: $h_r^2 = h_j^2 = 1/2$; $\psi = \pi/18$).

a Gaussian distribution, $\mathcal{N}(\mu_{pn} = 0, \sigma_{pn}^2 = 16 \times 10^{-4})$. We have also assumed RC oscillators, by considering the minimum achievable phase noise threshold, which is approximately -120 dBc/Hz [40]. For this case the oscillator phase-noise is also represented by a Gaussian distribution, $\mathcal{N}(\mu_{pn} = 0, \sigma_{pn}^2 = 16 \times 10^{-6})$. We simulated the phase-noise with a sample period $\Delta_T = T_c/360$ and $\phi(t)$ was added to the upconverted signal. Thus, instead of using (2) to compute the residual SI, we considered the phase noise and the residual SI was computed with the following formula

$$y_{r_{si}}(t) = h\, x_{si}(t-\tau) e^{j(\omega_c(t-\tau)+\phi(t-\tau))} - h_c\, x_{si}(t-\tau_c) e^{j(\omega_c(t-\tau_c)+\phi(t-\tau_c))}.$$

As can be seen in Fig. 6, the quality of the oscillators impacts on the distribution of the residual SI power. At the minimum achievable phase noise threshold (-120 dBc/Hz @ 1 MHz), the impact of the phase-noise on the distribution of the residual SI power is almost negligible. But, as the phase-noise increases (-100 dBc/Hz @ 1 MHz) the average of the residual SI power also increases.

V. CONCLUSIONS

A. APPLICABILITY OF THE PROPOSED APPROACH

It is well known that the knowledge of the residual SI due to the analog-domain cancellation is crucial to design efficient SI estimation methods to be used in the digital-domain. By doing so, the efficiency of the joint AC and DC schemes may be improved. The analytical derivation of the distribution of the residual SI power presented in this paper can be used to provide technical criteria for mitigating the SI residual interference in practical FDX communication systems. An obvious application is the compensation of the cancelation errors, which include the gain cancelation error $(1-\epsilon)$ and the phase cancellation error (ψ). By using the theoretical derivation presented in Section III and multiple samples of the residual SI collected in a practical FDX system, different estimation techniques can be employed to estimate the cancelation errors and compensate them (including but not limited to the method of moments[3]). However, the proposed derivation can also be useful for the academic community in general, to determine different aspects related with the performance analysis of FDX communications, including for example the capacity of FDX communication systems by using the residual SI power to derive the outage probability of a specific FDX system.

Finally, we highlight that although our work considers a single-tap delay channel, the approach may also be adopted in a multi-path scenario to provide an approximation of the residual SI. In FDX systems the LOS component is usually much higher than the non-LOS components (e.g. [42] reports 20-45 dBs higher). In this case, when the aggregated power of the non-LOS components is relatively low, our model can capture a significant amount of the residual SI power.

B. FINAL REMARKS

This work derives the distribution of the residual SI power due to channel estimation errors at the analog cancellation process. Closed form expressions were derived for the distribution of the residual self-interference power when Rician and Rayleigh fading self-interference channels are considered. Moreover, the distribution of the residual self-interference power was derived for low and high channel gain dynamics, by considering a time-invariant and a time-variant channel, respectively. The accuracy of the theoretical approach was assessed through Monte Carlo simulations for different levels of channel gain cancellation and phase errors during the channel estimation process. The results reported in the paper show that the channel dynamics strongly influence the distribution of the residual self-interference power. While for time-invariant channels the residual self-interference power

[3]In this case a channel estimation technique must also be employed to determine the channel statistics (h_j, h_r, σ_h, μ_h, or ϑ).

is exponentially distributed, for time-variant channels the exponential distribution is not a valid assumption. Instead, the distribution of the residual self-interference power in time-variant channels can be approximated by a product distribution, as described in Theorem 1, which constitutes the main contribution of this work.

REFERENCES

[1] D. Kim, H. Lee, and D. Hong, "A survey of in-band full-duplex transmission: From the perspective of PHY and MAC layers," *IEEE Commun. Surveys Tuts.*, vol. 17, no. 4, pp. 2017–2046, 4th quart., 2015.

[2] M. Heino *et al.*, "Recent advances in antenna design and interference cancellation algorithms for in-band full duplex relays," *IEEE Commun. Mag.*, vol. 53, no. 5, pp. 91–101, May 2015.

[3] Z. Zhang, X. Chai, K. Long, A. V. Vasilakos, and L. Hanzo, "Full duplex techniques for 5G networks: Self-interference cancellation, protocol design, and relay selection," *IEEE Commun. Mag.*, vol. 53, no. 5, pp. 128–137, May 2015.

[4] J. I. Choi, M. Jain, K. Srinivasan, P. Levis, and S. Katti, "Achieving single channel, full duplex wireless communication," in *Proc. 16th Annu. Int. Conf. Mobile Comput. Netw.*, New York, NY, USA, Sep. 2010, pp. 1–12.

[5] L. Wang, F. Tian, T. Svensson, D. Feng, M. Song, and S. Li, "Exploiting full duplex for device-to-device communications in heterogeneous networks," *IEEE Commun. Mag.*, vol. 53, no. 5, pp. 146–152, May 2015.

[6] S. Goyal, P. Liu, S. S. Panwar, R. A. Difazio, R. Yang, and E. Bala, "Full duplex cellular systems: Will doubling interference prevent doubling capacity?" *IEEE Commun. Mag.*, vol. 53, no. 5, pp. 121–127, May 2015.

[7] D. Kim, S. Park, H. Ju, and D. Hong, "Transmission capacity of full-duplex-based two-way ad Hoc networks with ARQ protocol," *IEEE Trans. Veh. Technol.*, vol. 63, no. 7, pp. 3167–3183, Sep. 2014.

[8] X. Xie and X. Zhang, "Does full-duplex double the capacity of wireless networks?" in *Proc. IEEE INFOCOM*, Toronto, ON, Canada, Apr. 2014, pp. 253–261.

[9] E. Ahmed and A. M. Eltawil, "All-digital self-interference cancellation technique for full-duplex systems," *IEEE Trans. Wireless Commun.*, vol. 14, no. 7, pp. 3519–3532, Jul. 2015.

[10] D. Korpi, L. Anttila, V. Syrjala, and M. Valkama, "Widely linear digital self-interference cancellation in direct-conversion full-duplex transceiver," *IEEE J. Sel. Areas Commun.*, vol. 32, no. 9, pp. 1674–1687, Sep. 2014.

[11] D. Korpi, T. Riihonen, V. Syrjälä, L. Anttila, M. Valkama, and R. Wichman, "Full-duplex transceiver system calculations: Analysis of ADC and linearity challenges," *IEEE Trans. Wireless Commun.*, vol. 13, no. 7, pp. 3821–3836, Jul. 2014.

[12] B. Debaillie *et al.*, "Analog/RF solutions enabling compact full-duplex radios," *IEEE J. Sel. Areas Commun.*, vol. 32, no. 9, pp. 1662–1673, Sep. 2014.

[13] J.-H. Lee, "Self-interference cancelation using phase rotation in full-duplex wireless," *IEEE Trans. Veh. Technol.*, vol. 62, no. 9, pp. 4421–4429, Nov. 2013.

[14] D. Bharadia and S. Katti, "Full duplex MIMO radios," in *Proc. 11th USENIX Symp. Netw. Syst. Design Implement.*, Seattle, WA, USA, Apr. 2014, pp. 359–372.

[15] L. Laughlin, M. A. Beach, K. A. Morris, and J. L. Haine, "Optimum single antenna full duplex using hybrid junctions," *IEEE J. Sel. Areas Commun.*, vol. 32, no. 9, pp. 1653–1661, Sep. 2014.

[16] E. Foroozanfard, O. Franek, A. Tatomirescu, E. Tsakalaki, E. De Carvalho, and G. F. Perdersen, "Full-duplex MIMO system based on antenna cancellation technique," *Electron. Lett.*, vol. 50, no. 16, pp. 1116–1117, Jul. 2014.

[17] P. Pursula, M. Kiviranta, and H. Seppa, "UHF RFID reader with reflected power canceller," *IEEE Microw. Wireless Compon. Lett.*, vol. 19, no. 1, pp. 48–50, Jan. 2009.

[18] D. Bharadia, E. McMilin, and S. Katti, "Full duplex radios," in *Proc. ACM SIGCOMM Conf.*, Hong Kong, Aug. 2013, pp. 375–386.

[19] R. Li, A. Masmoudi, and T. Le-Ngoc, "Self-interference cancellation with nonlinearity and phase-noise suppression in full-duplex systems," *IEEE Trans. Veh. Technol.*, vol. 67, no. 3, pp. 2118–2129, Mar. 2018.

[20] A. Sahai, G. Patel, C. Dick, and A. Sabharwal, "Understanding the impact of phase noise on active cancellation in wireless full-duplex," in *Proc. 46th Conf. Rec. Asilomar Conf. Signals, Syst. Comput. (ASILOMAR)*, Nov. 2012, pp. 29–33.

[21] M. Duarte, "Full-duplex wireless: Design, implementation and characterization," Ph.D. dissertation, Dept. Elect. Computer Eng., Rice Univ., Houston, TX, USA, 2012.

[22] A. Masmoudi and T. Le-Ngoc, "A maximum-likelihood channel estimator for self-interference cancelation in full-duplex systems," *IEEE Trans. Veh. Technol.*, vol. 65, no. 7, pp. 5122–5132, Jul. 2016.

[23] A. Sahai, G. Patel, C. Dick, and A. Sabharwal, "On the impact of phase noise on active cancelation in wireless full-duplex," *IEEE Trans. Veh. Technol.*, vol. 62, no. 9, pp. 4494–4510, Nov. 2013.

[24] S. Li and R. D. Murch, "An investigation into baseband techniques for single-channel full-duplex wireless communication systems," *IEEE Trans. Wireless Commun.*, vol. 13, no. 9, pp. 4794–4806, Sep. 2014.

[25] M. Sakai, H. Lin, and K. Yamashita, "Adaptive cancellation of self-interference in full-duplex wireless with transmitter IQ imbalance," in *Proc. IEEE GLOBECOM*, Dec. 2014, pp. 3220–3224.

[26] E. Ahmed and A. M. Eltawil, "On phase noise suppression in full-duplex systems," *IEEE Trans. Wireless Commun.*, vol. 14, no. 3, pp. 1237–1251, Mar. 2015.

[27] V. Syrjala, M. Valkama, L. Anttila, T. Riihonen, and D. Korpi, "Analysis of oscillator phase-noise effects on self-interference cancellation in full-duplex OFDM radio transceivers," *IEEE Trans. Wireless Commun.*, vol. 13, no. 6, pp. 2977–2990, Jun. 2014.

[28] M. Duarte, C. Dick, and A. Sabharwal, "Experiment-driven characterization of full-duplex wireless systems," *IEEE Trans. Wireless Commun.*, vol. 11, no. 12, pp. 4296–4307, Dec. 2012.

[29] Y.-S. Choi and H. Shirani-Mehr, "Simultaneous transmission and reception: Algorithm, design and system level performance," *IEEE Trans. Wireless Commun.*, vol. 12, no. 12, pp. 5992–6010, Dec. 2013.

[30] M. Duarte *et al.*, "Design and characterization of a full-duplex multiantenna system for WiFi networks," *IEEE Trans. Veh. Technol.*, vol. 63, no. 3, pp. 1160–1177, Mar. 2014.

[31] T. Riihonen, S. Werner, and R. Wichman, "Mitigation of loopback self-interference in full-duplex MIMO relays," *IEEE Trans. Signal Process.*, vol. 59, no. 12, pp. 5983–5993, Dec. 2011.

[32] B. P. Day, A. R. Margetts, D. W. Bliss, and P. Schniter, "Full-duplex MIMO relaying: Achievable rates under limited dynamic range," *IEEE J. Sel. Areas Commun.*, vol. 30, no. 8, pp. 1541–1553, Sep. 2012.

[33] L. Irio, R. Oliveira, and L. Oliveira, "Characterization of the residual self-interference power in full-duplex wireless systems," in *Proc. IEEE Int. Symp. Circuits Syst.*, Florence, Italy, May 2018, pp. 1–5.

[34] A. Masmoudi and T. Le-Ngoc, "Self-interference cancellation limits in full-duplex communication systems," in *Proc. IEEE Global Telecomm. Conf.*, Washington, DC, USA, Dec. 2016, pp. 1–6.

[35] X. Li, C. Tepedelenlioğlu, and H. Şenol, "Channel estimation for residual self-interference in full-duplex amplify-and-forward two-way relays," *IEEE Trans. Wireless Commun.*, vol. 16, no. 8, pp. 4970–4983, Aug. 2017.

[36] A. Nadh, J. Samuel, A. Sharma, S. Aniruddhan, and R. K. Ganti, "A Taylor series approximation of self-interference channel in full-duplex radios," *IEEE Trans. Wireless Commun.*, vol. 16, no. 7, pp. 4304–4316, Jul. 2017.

[37] L. Samara, M. Mokhtar, Ö. Özdemir, R. Hamila, and T. Khattab, "Residual self-interference analysis for full-duplex OFDM transceivers under phase noise and I/Q imbalance," *IEEE Commun. Lett.*, vol. 21, no. 2, pp. 314–317, Feb. 2017.

[38] A. Shojaeifard, K.-K. Wong, M. Di Renzo, G. Zheng, K. A. Hamdi, and J. Tang, "Self-interference in full-duplex multi-user MIMO channels," *IEEE Commun. Lett.*, vol. 21, no. 4, pp. 841–844, Apr. 2017.

[39] L. Irio and R. Oliveira, "On the impact of fading on residual self-interference power of in-band full-duplex wireless systems," in *Proc. 14th Int. Wireless Commun. Mobile Comput. Conf. (IWCMC)*, Limassol, Cyprus, Jun. 2018, pp. 142–146.

[40] R. Navid, T. H. Lee, and R. W. Dutton, "Minimum achievable phase noise of RC oscillators," *IEEE J. Solid-State Circuits*, vol. 40, no. 3, pp. 630–637, Mar. 2005.

[41] D. Wulich, N. Dinur, and A. Glinowiecki, "Level clipped high-order OFDM," *IEEE Trans. Commun.*, vol. 48, no. 6, pp. 928–930, Jun. 2000.

[42] E. Everett, A. Sahai, and A. Sabharwal, "Passive self-interference suppression for full-duplex infrastructure nodes," *IEEE Trans. Wireless Commun.*, vol. 13, no. 2, pp. 680–694, Jan. 2014.

[43] S. Abdollahvand, J. Goes, L. B. Oliveira, L. Gomes, and N. Paulino, "Low phase-noise temperature compensated self-biased ring oscillator," in *Proc. IEEE Int. Symp. Circuits Syst.*, Seoul, South Korea, May 2012, pp. 2489–2492.

LUIS IRIO received the M.Sc. degree in electrical and computer engineering from the Nova University of Lisbon, in 2013, where he is currently pursuing the Ph.D. degree in electrical and computer engineering. From 2014 to 2015, he was a Researcher at CTS-UNINOVA. He is currently a Researcher with the Instituto de Telecomunicações. His research interests include full-duplex systems, multi-packet reception systems, and wireless mobile systems.

RODOLFO OLIVEIRA (S'04–M'10–SM'15) received the Licenciatura degree in electrical engineering from the Faculdade de Ciências e Tecnologia (FCT), Universidade Nova de Lisboa (UNL), Lisbon, Portugal, in 2000, the M.Sc. degree in electrical and computer engineering from the Instituto Superior Técnico, Technical University of Lisbon, in 2003, and the Ph.D. degree in electrical engineering from UNL, in 2009. From 2007 to 2008, he was a Visiting Researcher with the University of Thessaly. From 2011 to 2012, he was a Visiting Scholar at Carnegie Mellon University. He is currently with the Department of Electrical and Computer Engineering, UNL, and is also a Senior Researcher with the Instituto de Telecomunicações, where he researches in the areas of wireless communications, computer networks, and computer science. He serves in the Editorial Board of *Ad Hoc Networks* (Elsevier).